This is a preproof accepted article for *Annals of Glaciology*
This version may be subject to change during the production process
DOI: 10.1017/aog.2025.10014

Constraining Snow Water Equivalent of Wet Snowpacks in Southeast Alaska

Mikaila Mannello[1,2*], Scott Braddock[1,2], Seth Campbell[1,2], Emma Skelton[1,2,3], Kristin M. Schild[1,2], Christopher McNeil[4]

[1] Climate Change Institute, University of Maine, ME, USA
[2] School of Earth and Climate Science, University of Maine, ME, USA
[3] Cold Regions Research and Engineering Laboratory, Hanover, NH, USA
[4] U.S. Geological Survey Alaska Science Center, Anchorage, AK, USA
*Correspondence: Mikaila Mannello (mikaila.mannello@maine.edu)

Abstract. Quantifying snow water equivalent (SWE) with ground-penetrating radar (GPR) in a warming climate is complicated by the incidence and variability of liquid water in snow. Snow surveys conducted during the melt season serve as a valuable analog to conditions under future warming. Here, we determine the variability of wet snowpack properties (relative permittivity and density) to quantify their impact on SWE estimates using GPR. We collected spatially continuous snowpack measurements with 400 MHz GPR in 2012 and 2021 across repeat transects (~150 km each year) along with spring and summer snow depth and density measurements from snow pits and snow cores. Snow relative permittivity values ranged between 2.06 – 2.62 in 2012 and 2.11 – 5.11 in 2021, resulting in calculated volumetric liquid water content (LWC) between 1.7% – 5.7% in 2012 and 2.1% – 16% in 2021. This variability in snow relative permittivity results in SWE uncertainties between 8% – 33%, with more extreme cases reaching 13% – 45%. We attribute this uncertainty to spatial and temporal variability in liquid water content when using GPR to estimate SWE. As snowpacks become wetter with rising atmospheric temperatures, GPR surveys should include in-situ relative permittivity measurements to reduce depth and SWE interpretation uncertainties.

1. Introduction

Quantifying snow water equivalent (SWE) is crucial for assessing the annual mass balance of glaciers, water resources, and potential glacier contributions to sea-level rise. Ground-penetrating radar (GPR) offers a valuable quantitative, non-destructive method to estimate SWE along profiles tens to hundreds of kilometers long within a single field season, accounting for variability of snow distribution across larger areas (e.g., Bradford and others, 2009; McGrath and others, 2015; McGrath and others, 2018). Often studies conduct surveys early in the year (spring), avoiding the impact of liquid water content (LWC), simplifying assumptions of radar wave velocity when determining snow depth. However, research suggests that the sub-Arctic and Arctic are already rapidly warming (Winski and others, 2018; Ballinger and others, 2023) and are projected to continue doing so, leading to earlier spring snowmelt onset (Zheng and others, 2022), more incidences of rain-on-snow events (Pan and others, 2018), and greater contributions from glaciers to global sea-level rise (Oerlemans and others, 2005; Rounce and others, 2023). Given this trend, assessments of wet snowpacks for SWE will likely become more common. Therefore, our aim is to determine the variability of wet snowpack properties and quantify their impact on SWE estimates using GPR and ground-truth methods.

Most data related to our understanding of mass balance and SWE on Alaskan glaciers come from smaller U.S. Geological Survey (USGS) Benchmark glaciers (areas <20 km^2) (McGrath and others, 2018; O'Neel and others, 2019) with few results from larger glaciers (e.g. McGrath and others, 2015). McGrath and others (2015) used GPR surveys across seven glaciers and five climate regions and find that SWE across Alaskan glaciers is highly variable, and heavily influenced by wind-shading, elevation, and storm track trajectory. Further, they find that accumulation rates derived from radar exceed those estimated by glaciological methods, and that there is significant SWE variability along those centerlines. This included a small survey (several kilometers) on Taku Glacier, suggesting that there is limited spatial variability in end-of-winter SWE on Taku Glacier and greater variability on other Alaskan glaciers in their study.

Determining snow depth and SWE with GPR requires knowledge of the radar wave velocity traveling through the snowpack. Typically, this velocity is assumed to be spatially or temporally homogeneous. Many studies have addressed this limitation by applying a density-dependent bulk radar wave velocity across the study area (e.g., Gascon and others, 2013; Miège and others, 2013; Sold and others, 2015; McGrath and others, 2018). However, since radar wave velocity is affected by snowpack density and strongly affected by LWC, both properties that can vary in space and time, this assumption can lead to uncertainty in SWE estimates. Understanding how density and LWC vary spatially is therefore crucial to interpretations of snow depth and calculating SWE from GPR observations. Several recent studies focused on evaluating the effects of density and LWC on radar wave velocity. For example, St. Clair and Holbrook (2017) used migration velocity analysis with common-offset radar to determine the most appropriate velocity for a dry snowpack in Wyoming. Recent work in seasonal snowpacks used GPR in combination with destructive (e.g., snow pits and dye tracing) and non-destructive methods (e.g., terrestrial Light Detection and Randing, airborne imagery, and Structure from Motion) for assessing and monitoring spatial variations in seasonal snowpack depth, density, SWE, and volumetric LWC throughout the springtime (Webb and others, 2018; Webb and others, 2019; Bonnell and others, 2021; McGrath and others, 2022; Webb and others, 2022; Bonnell and others, 2023). These studies find that LWC can vary spatially (Webb and others, 2018; Bonnell and others, 2023), diurnally (Bonnell and others, 2021) and seasonally (Schmid and others, 2015). Other approaches have implemented multiple antenna configurations to determine radar wave velocities of snow and firn layers. Examples include common mid-point (CMP) surveys on annual accumulation (McGrath and others, 2015) and multi-offset radar on seasonal snowpacks (Greissinger and others, 2018) and on polar firn (Meehan and others, 2021). Our work applies an approach most similar to Bonnell and others (2021) using in-situ snow depths to calculate snow LWC.

With continued warming, we expect the window of dry snow to shorten and further work is necessary to better constrain LWC and SWE variations in wet snowpacks to expand the time to capture winter accumulation across large spatial areas. Here, we utilize 400 MHz common-offset GPR surveys in conjunction with in-situ snow depth and density measurements to further constrain and assess the impact of wet snow properties on SWE estimates across the Juneau Icefield (JIF) in Southeast Alaska (Figs. 1, S1). We calculate bulk radar wave velocity in 2012 and 2021 at a total of 13 locations with GPR surveys and ground-truth snow depths from snow pits and cores. We then combine these calculations with dry (spring) snow density measurements to quantify the variability in LWC across the study site. Density measurements collected from 31 summer snow pits on JIF in 2012 and 2021 are combined with snow depth interpretations from repeat 400 MHz common-offset GPR surveys to calculate bounds of the range of SWE across JIF in July 2012 and 2021. We estimate variability in relative permittivity and LWC within the snowpack and the resulting uncertainties SWE estimates, constrained by in-situ snow density and depth measurements.

2. Study Site

2.1. Juneau Icefield, Alaska

JIF (Fig. 1), one of Alaska's largest icefields, is currently losing mass with increased warming (McNeil and others, 2020) averaging 5.9 ± 0.8 km^3 a^{-1} in volume loss between 2010 – 2020

(Davies and others, 2024). Taku Glacier (725 km^2), traditionally named T'aak̲ú K̲wáan Sít'i (the T'aak̲ú peoples' glacier (Thornton, 2010)) is the main outlet drainage of the southern portion of JIF (McNeil and others, 2021). Since 1946, rates of annual mass loss have increased in correlation with increasing mean summer temperatures (McNeil and others, 2020). ERA5-Land 2m temperature data (Muñoz, 2019) indicates a warming of 0.28˚C per decade over the JIF region (58 – 59.3°N, 133.2 – 135°W) between 1950 and 2024 and with average yearly temperatures more frequently approaching 0˚C (Supplementary S.2.). JIF receives between 2.5 – 4.4 m w.e. of winter (October – March) precipitation each year (Roth and others, 2018) and experiences prevalent melt during summer months (JJA) producing supraglacial melt ponds and streams in both the accumulation and ablation zones. The established field stations and annual field campaigns of the Juneau Icefield Research Program (JIRP) provide ideal access and logistical support to enable extensive GPR surveys and ground-truth efforts during peak warming (and increased snow water content) months.

3. Methods

3.1. Ground-Penetrating Radar

To assess the impact of LWC on SWE from GPR, we analyzed approximately 150 km of GPR surveys collected across JIF in July 2012 and in July 2021, following the 2012 GPS tracks for repeatability (Fig. 2) (Campbell, 2024). Surveys covered 8 catchment basins and elevations from ~1000 – 1800 m, providing data to encompass the spatial variability of snowpack depth, LWC, and SWE. We conducted these surveys by towing a Geophysical Survey Systems Incorporated (GSSI) control unit (SIR-3000 in 2012; SIR-4000 in 2021) and Garmin GPSMap handheld units for georeferencing (see Supplementary S.3. for detailed processing) coupled with a GSSI model 5103 400 MHz antenna on a plastic sled at 3 – 7 km h^{-1} via snow machine. Surveys were conducted along the centerline of several branches of Taku Glacier and along 3 cross-sections (Fig. 1).

Figure 1 near here

GPR data were collected with a time window of 250 – 400 ns, 2048 samples per trace, 24 traces per second, and were not stacked during collection. The sampling rate and towing speeds of 3 – 7 km h^{-1} yield traces at 3.5 – 8.1 cm intervals across the profiles. After collection, all GPR profiles were time-zero corrected, distance normalized, and stacked 10- to 30-fold using GSSI's proprietary software, RADAN v.7. Some profiles were filtered with low- and high-pass filters (800 MHz and 100 MHz, respectively) if noise was apparent in the radargrams. However, the data quality was generally high, so no other filtering or processing was required. We identified the annual accumulation – firn boundary as the most spatially continuous horizontal reflection horizon across both the ablation and accumulation zones (Fig. 2) and converted the GPR two-way travel time (TWTT) data to annual snow accumulation depth (*z*) with:

$$z = \frac{TWTT \cdot v}{2} \tag{1}$$

where the bulk average velocity *v* of the radar wave through the snowpack is given by

$$v = \frac{c}{\sqrt{\varepsilon_s}} \tag{2}$$

where *c* is the speed of light (0.3 m ns^{-1}) and ε_s is the relative permittivity of snow.

3.2. Ground-truth Snow Depth & Relative Permittivity

In this study, ε_s is determined by

$$\varepsilon_s = \left(\frac{c \cdot TWTT_{gt}}{2z_{gt}}\right)^2 \tag{3}$$

using ground-truth measurements of depth (z_{gt}), measured by snow pit and snow core depths located within 25 m of the GPR survey and TWTT of the accumulation layer at the ground-truth site ($TWTT_{gt}$). The latter are derived from the stacked profile, thus utilizing the average of the closest 10-30 original scans, where GPR transects passed at a distance of 3 – 24 m from each ground-truth site to both capture the local accumulation and also minimize potential reflections from the snow pit wall itself (Fig. 2). Sensitivity tests were performed on these single $TWTT_{gt}$ picks compared to the average picks over 50 m and the average of 25 traces nearest to the ground-truth site to validate our use of $TWTT_{gt}$ for ε_s calculations (Supplementary S.4., Table S1).

Figure 2 near here

The snow pits used for ground-truth snow depth were selected from a dataset collected by JIRP during summer mass balance surveys (Campbell, 2024). Additional ground-truth snow depths were collected in 2021 with a Kovacs Mark II Coring System. GPR surveys and ground-truth snow depth measurements were obtained concurrently whenever possible but, due to the time required to dig snow pits, this was not possible for 3 sites in 2012. For these cases, we applied a surface correction using ablation stake measurements (Table 1; see Supplementary S.5.). Additionally, we assessed the relationship between ε_s and lapse-rate derived air temperature (see Supplementary S.6.).

Table 1 near here

3.3. Liquid Water Content

We calculated the volumetric LWC of the snowpack at each ground-truth location using an empirical relationship between dry snow density (ρ_d), volumetric liquid water content (W_v), and relative permittivity of dry, wet, and measured snow (ε_d, ε_w, ε_s) (Tuiri and others, 1984; Sihvola and Tuiri, 1986):

$$\varepsilon_s = (0.10W_v + 0.80W_v^2)\varepsilon_w + \varepsilon_d \tag{4}$$

where the permittivity of dry snow is defined by Tuiri and others (1984) as:

$$\varepsilon_d = 1 + 1.7\rho_d + 0.7{\rho_d}^2 \tag{5}$$

For all LWC calculations we used a single value for ρ_d of 0.444 g cm^{-3}, estimated by averaging spring snow densities collected across JIF in 2013-2015 (ranging between 0.400 g cm^{-3} to 0.550 g cm^{-3}; McNeil and others, 2017; O'Neel and others, 2017) and used a value of 88 for ε_w for water at the freezing point. Although these densities were collected outside of the study years, we assume these measurements are representative of dry snow density for this snowpack because of the documented consistency in the summer wet snow density across JIF (LaChapelle, 1954; Pelto and Miller, 1990; McNeil and others, 2020).

3.4. Snow Water Equivalent

We calculated SWE across JIF using GPR and all available density measurements from JIRP's mass balance program in 2012 and 2021 (Pelto and others, 2013; McNeil and others, 2020), including data from nearby or adjoining glaciers such as Lemon Creek Glacier and Tulsequah Glacier (Fig. 1). These snow depth and wet snow density measurements were from a total of 18 and 13 snow pits in 2012 and 2021, respectively; typically, snow pit depths reached between 300 – 500 cm. Density measurements were sampled from the north-facing wall of each pit at 10 cm intervals using a 500 cm^3 sampling cylinder. Any observable ice lenses or ice pipes over 0.2 cm through the snowpack were recorded. For each study year, density data from all snow pits were aggregated and averaged within each 10 cm depth interval to yield the average and standard deviation of wet density (ρ_w) at each depth interval across JIF, and an exponential equation was fit to all the density data for each study year ($\rho_w(z)$) (Fig. S4).

Because using snow depth-dependent density calculations reduce errors in calculating SWE (Lundberg and others, 2006), we calculated SWE along the JIF profiles by integrating the exponential relation derived above, $\rho_w(z)$, from the surface (z = 0) to the snowpack depth (z = d) to capture the density differences throughout the snow column with:

$$SWE = \int_0^d \rho_w(z)dz \tag{6}$$

For the two study years, SWE was calculated using snow depths from mean ($\overline{\varepsilon_s}$ ± 1 s.d.), minimum ($\varepsilon_{s,min}$), and maximum ($\varepsilon_{s,max}$) relative permittivity in each year to provide bounds on SWE for the range of observed conditions.

4. Results

4.1. Relative Permittivity and Liquid Water Content

Relative permittivity and LWC (% volume) estimates show variability across the study region, with no consistent trend between 2012 and 2021 (Figs. 3, 4). Using the 13 ground-truth sites, estimates of ε_s range from 2.06 – 2.62 in 2012 ($\overline{\varepsilon_s} = 2.48 \pm 0.20$) and from 2.11 – 5.11 in 2021 ($\overline{\varepsilon_s} = 3.56 \pm 1.07$) (Fig. 3, Table 1). Uncertainty in relative permittivity is 0.106, calculated using mean $TWTT_{gt}$ (50.93 ns) and mean snow depth (447 cm) (see Supplementary S.8.). Using the calculated ε_s, LWC estimates range between 1.7% – 5.7% in 2012 (avg. 4.8%), and from 2.1% – 16% in 2021 (avg. 9.6%). While higher elevations exhibited higher relative permittivity values, no dominant spatial trend was observed (Fig. 3). Additionally, LWC values were not consistent between years, nor is there a consistent trend at the same locations (Figs. 4, S5).

Figure 3 near here

Figure 4 near here

4.2. GPR-derived Snow Depths

The average TWTT for the accumulation layer across all radar transects was 51.1 (±16.3) ns in 2012 and 44.5 (±17.8) ns in 2021. For 2012 depth calculations, we used $\overline{\varepsilon_s}$ of 2.48 (ρ_d= 0.444 g cm^{-3}, W_v = 4.8%), resulting in an average annual accumulation depth of 524 cm ± 153 cm. In

2021, the $\overline{\varepsilon_s}$ of 3.56 (ρ_d= 0.444 g cm^{-3}, W_v = 9.6%) applied across the dataset resulted in an average annual accumulation depth of 351 cm ± 138 cm.

4.3. Snow Pit Density and Snow Water Equivalence Estimates

To calculate SWE, we established the average wet snow density curves using all available snow pits collected in 2012 and 2021, consisting of 18 snow pits in 2012 and 13 snow pits in 2021 (Figs. 1, S4). Snow pit densities were relatively consistent between years, averaging 0.556 ± 0.030 g cm^{-3} in 2012 (avg. depth 552 ± 94 cm) and 0.562 ± 0.025 g cm^{-3} in 2021 (avg. depth 422 ± 88 cm). Snow density follows the expected trend of increasing density with depth (Fig. S4). Equations describing the relationship between density and depth for each year are $\rho_{w,2012}(z) = 0.403z^{0.06}$ (R^2 = 0.86) and $\rho_{w,\,2021}(z) = 0.450z^{0.04}$ (R^2 = 0.66).

Using GPR-derived snow depths and density data, we calculated average SWE to be 286 ± 89 cm w.e. ($\overline{\varepsilon_s}$ = 2.48) in 2012 and the average SWE in 2021 to be 193 ± 80 cm w.e. ($\overline{\varepsilon_s}$ = 3.56) (Fig. 5), representing a -32% change between 2012 and 2021 (see Supplementary S.7. for ice lens considerations). However, there is high spatial variability in ε_s in 2021, which we infer to be due to the variability in LWC. We therefore calculated the range of SWE possible in each year based upon the minimum and maximum calculated relative permittivity for each year ($\varepsilon_{s,min},\ \varepsilon_{s,max}$) and find a potential 13% difference in mean SWE in 2012 and a 45% difference in mean SWE in 2021 (Table 2). Acknowledging those are the maximum differences, we also calculated the potential difference in mean SWE for $\overline{\varepsilon_s}$ ±1 s.d. to be 8% and 33% in 2012 and 2021, respectively.

Figure 5 near here

Table 2 near here

5. Discussion

5.1. Spatial and Temporal Variability in Relative Permittivity and LWC

Spatial variability in ε_s across JIF was lower in 2012 relative to 2021 (Fig. 3). Previous studies have documented spatial variability in relative permittivity, e.g. in seasonal snowpacks in Colorado and Montana, where measured permittivity values range between ~1.3 – 2.4 (Webb and others, 2022) and were calculated to be ~1.4 – 1.6 (Bradford and others, 2009), and ~1.5 – 2.5 (Bonnell and others, 2023). The range of ε_s in 2012 calculated here (2.06 – 2.62) is slightly greater than but more similar to ε_s measured in those seasonal snowpacks than the range in 2021 (2.11 – 5.11). In this glaciological setting, differences in relative permittivity are primarily due to differences in density and LWC. In this way, we attribute the wider range of ε_s reported here to, in part, the greater wet snow density observed on JIF (0.460 – 0.600 g cm^{-3}) when compared to these seasonal snow studies (~0.230 – 0.500 g cm^{-3}), but more likely attribute this to differences in LWC.

Observed density patterns across JIF (Section 4.3) are similar to those previously reported at this location (LaChapelle, 1954; Pelto and Miller, 1954). Since densification takes weeks to months, while meltwater production and percolation occur on timescales of hours to days, and our results include permittivity values greater than that of glacier ice (3.15), we attribute the variability of calculated relative permittivity in 2012 and 2021 to LWC within the snowpack. LWC values calculated here are spatially and temporally variable, ranging between 1.7 – 16% (by volume), similar to the range presented in by Webb and others (2018) for seasonal snowpacks (0 – 19%). On a smaller spatial scale, Techel and Pielmeier (2011) carried out snow fork surveys in the Swiss Alps to demonstrate spatial variability in LWC of 0 – 10% (by volume) in a 5 m wide by 80 cm deep snow pit. LWC results presented here agree with the findings of spatial (Webb and others, 2018) and temporal variability (Techel and Pielmeier, 2011) in LWC.

In addition to spatial variability in ε_s and LWC, there is also likely substantial temporal variability of meltwater in this snowpack during the summer months, a time of high ablation and rain-on-snow events. Colbeck (1975) modeled how different snowpacks respond to rain-on-snow events and finds water moves fastest though an isothermal snowpack, as compared to fresh snow or refrozen snow. Temporal variability in ε_s and LWC in snow is found to vary diurnally, between days, and between seasons in seasonal snowpacks (Techel and Pielmeier, 2011; Schmid and others, 2015; Bonnell and others, 2021) and on a glacier in Western Norway (Hart and others, 2011). Bonnell and others (2021) similarly observed spatial and temporal variability in LWC in a seasonal snowpack between April to June in Colorado with LWC values remaining low in the spring and increasing during the summer with some areas reaching >10% LWC. In our study, there was not a consistent trend of an increase or decrease in ε_s at sites repeated in both years, agreeing with this temporal variability observed elsewhere (Figs. 3, 4).

Values of ε_s in this study are higher than most other ground-truthed GPR studies on glaciers, which are typically conducted in spring, whereas our data were collected in mid-July during a time when temperatures are consistently above freezing and precipitation may fall as rain. Clayton (2022) conducted a snowpack meltwater percolation study on JIF, near the Matthes-Llewellyn ice divide (~1800 m), in 2018 and 2019 and observed the movement of meltwater within this snowpack on sub-daily timescales and trends indicative of diurnal melting and refreezing. In a dense and isothermal snowpack such as on JIF, we expect surface melt or rain to move through the snowpack, but this can be impeded by ice lenses. Evidence of ice lensing on JIF supports the idea that there are meltwater or rain events where water percolates deeper into the snowpack before refreezing into an ice lens. Previous work has demonstrated horizontal hydrological connectivity in snowpacks and the effect of snowpack layering and ice lenses on vertical meltwater movement (Webb and others, 2019; Webb and others, 2022). It is likely that the ice lenses within the snow impact this water movement and result in increased snow permittivity. Here, the heterogeneity of ice lensing and water movement through snowpacks may additionally help explain such varied and high values of ε_s on JIF.

Spatial variability in the LWC varies depending on the time of day of radar transects (Webb and others, 2018; Bonnell and others, 2021) and the prior meteorological conditions (Hart and others, 2013). In both 2012 and 2021, the average temperature during the days of data collection was above freezing (8.17 ± 1.43 ˚C and 7.21 ± 0.91 ˚C, respectively) at 1196 m on JIF from lapse-rate derived temperatures (Supplementary S.6., Fig. S3). However, there is not a strong correlation between relative permittivity and air temperature in either year. Some of the high variability in the 2021 data and low variability in the 2012 data may be attributed to precipitation (or lack thereof), but there are no in-situ continuous precipitation data available for this study site, and the meteorological data from the Juneau International Airport is too localized to represent precipitation on JIF. It is possible that differences in precipitation and solar insolation contribute to this difference in water content between years, but this cannot be ascertained with the present data. Therefore, this is an area of study that should be investigated in future work.

5.2. Snow Water Equivalent

The GPR surveys still show patterns that are a result of climatological and topographical factors such as elevation and proximity to the moisture source. We observe SWE gradients with elevation of 30 cm/100 m (R^2 = 0.46) in 2012 and 21 cm/100 m (R^2 = 0.26) in 2021, computed with $\overline{\varepsilon_s}$ for each year. (Fig. S6 (a, c)). These values are within the range of accumulation gradients presented in McNeil and others (2020) from over 20 years of JIF data, and similar to values found by McGrath and others (2015) ranging between 11.5 – 40.0 cm/100 m for glaciers near the Gulf of Alaska. The impact of elevation may be amplified on marine-proximal glaciers, where the high-elevation areas are also those closest to the coast and therefore receive more precipitation than interior regions of JIF. We observe an inverse relationship between distance from the coastline and snow accumulation depth and SWE of -7 cm km^{-1} ($R^2 = 0.24$) in 2012 and -9 cm km^{-1} ($R^2 = 0.46$) in 2021 (Fig. S6 (b, d)). These trends are most notable for more coastal branches of JIF, in agreement with a comparison between Lemon Creek Glacier and Taku Glacier in McNeil and others (2020). These results also support the modeling presented in Roth and others (2018) who find that the area of JIF closest to the coastline has the highest winter precipitation and aligns with the wind direction most dominant between October and March.

While these results align within expected values and trend direction, the magnitude of these relationships are impacted by the applied ε_s, either being amplified or diminished (Tables S2-S3). Both the conservative (8% – 33%) and extreme (13% – 45%) differences in mean SWE from GPR due to different ε_s indicate the potential for over- or underestimation in mass balance and water resources. Due to the lack of spatial trends in ε_s, it is not possible at this time to establish these relationships more accurately. The implications of this may either steepen or lessen mass balance gradients and support the need for resolving ε_s and LWC variations at higher spatial and temporal resolution.

5.3. Survey Implications in a Warming Climate

The onset of snowmelt across Alaska is occurring earlier in the spring due to increasing atmospheric temperatures (Zheng and others, 2022). Ballinger and others (2023) showed that between 1957-2021, the Central Panhandle of Alaska, which includes JIF, experienced a -3.13% change in snowfall equivalent per decade and increases in 2 m air temperature in every season (Ballinger and others, 2023). Under modeled future warming scenarios, southeastern Alaska is predicted to experience warmer temperatures and less precipitation (Bigalke and Walsh, 2022). Alaskan glacier systems are amongst those predicted to lose mass and contribute the most to global sea-level rise in the next century (Oerlemans and others, 2005; Rounce and others, 2023). With warmer seasons throughout the year, JIF could experience an earlier onset of melt or more predominant spatial and temporal variability in LWC. In this way, perhaps even spring surveys of SWE using GPR should consider increasing the spatial and temporal sampling density of ground-truth snow depths for accurate interpretations.

These trends extend beyond Southeast Alaska, with broader implications for other areas in Alaska and for areas of the Arctic that typically have dry snow. Temperatures are rising faster at the poles than at mid-latitudes, especially in the Northern Hemisphere (Holland and Bitz, 2003). Rain-on-snow events recently occurred at Summit Station, Greenland (Xu and others, 2022) and predicted to occur under future warming scenarios in Svalbard (Hansen and others, 2014). Such changes may require accounting for LWC variability considerations in areas that historically have dry snowpacks.

The spatial variability in ε_s and, by implication, LWC presented here supports the need for an increased sampling density of ground-truth points. This study demonstrated a large spatial variability in LWC (2.1% – 16% in 2021), even within 7 to 10 days, which negates the assumption that conditions are homogenous across a large (>500 km^2) study site. Variations of LWC occur on annual, daily, or even shorter timescales, and the degree of variability between the survey years at the same location demonstrates that we cannot assume the same conditions between years even if surveys occur at the same time as years prior. Understanding more about the spatial and temporal variability of meltwater in snow helps us potentially expand the window for data collection of SWE with GPR if we can properly account for the water.

To remedy this situation, we recommend ground-truth points via snow pits or coring at least at the end-point of GPR surveys and potentially in the middle of survey lines if there are substantial changes in topography along the transect, such as more than 300 m of elevation change, rolling topography, or sudden increases or decreases in topographic wind shading. Examples of factors which may spatially and temporally influence snowpack relative permittivity include (but are not limited to) elevation change, aspect, and solar barriers such as nunataks (which may shield the sun and reduce melt). Newer techniques including multi-offset radar may mitigate some of these limitations where the antenna configuration consisting of multiple transmitters and receivers can continuously derive the layer radar wave velocity across the survey (Bradford and others, 2009; Greissinger and others, 2018; Meehan and others, 2021). Future research should consider annual surveys, sub-seasonal surveys, and the use of multi-offset radar to better quantify these trends and variability.

6. Conclusions

In this study, we analyzed two years of 150 km GPR surveys with ground-truth points from snow pits and snow cores in 2012 and 2021 to assess the variability of summer snowpack ε_s on JIF. We calculated LWC at each ground-truth location using an empirical relation to infer snowpack LWC ranging from 1.7 – 16%. Finally, we provided bounds on the SWE across JIF in 2012 and 2021 using density data from 31 summer snow pits and the calculated $\varepsilon_{s,max}$, $\varepsilon_{s,avg}$, $\varepsilon_{s,min}$ from 13 ground-truth points across JIF. We find that depth-density trends across JIF within and between years are relatively consistent and that, across the range of calculated ε_s, differences in interpreted depths due to ε_s introduce substantial uncertainty to SWE calculations (8% – 33%, with extreme cases of 13% – 45%) by GPR.

GPR is an effective, non-destructive tool to rapidly extend point-based measurements of SWE across large spatial extents (10s to 100s of kms). However, in wet snow environments, GPR assumptions about relative permittivity must be made with caution. Our results show that SWE estimates from GPR in such conditions require extensive ground-truth campaigns due to the spatial and temporal variability in snowpack LWC. As airborne and ground-based radar surveys become more common in high-latitude glacier and ice sheet studies, the expected increase in LWC due to rising temperatures may complicate GPR interpretation especially in Alaska, western Canada, and polar areas. To ensure accurate interpretations of depth and SWE, ground-truth campaigns should be conducted as close in time as possible to the time of surveying and across the broadest spatial scale feasible. Future work should aim to resolve this LWC variability at higher spatial and temporal resolution to improve SWE estimates.

Supplemental Information

The supplementary material for this article is available at (doi placed here when available)

Data Availability

GPR and Summer Snow Pit Data available through the Arctic Data Center (Campbell, 2024).

Spring Snow Density Data available through U.S. Geological Survey data release (McNeil and others, 2017).

NWS NOAA NOWData Meteorological Data publicly available at: https://www.weather.gov/wrh/Climate?wfo=ajk

Author Contribution

MM conducted data processing, data analysis, and initial writing and revising the manuscript. SB conducted both years of data collection, preliminary data processing, and revisions to the manuscript. SC provided funding acquisition, supervision, idea conceptualization, both years of data collection, software resources, and provided extensive revisions. ES conducted the second year of data collection and provided feedback on revisions. KS contributed guidance on data analysis and revisions. CM provided advice and interpretations of snow pit ground-truth data.

Acknowledgements

We are grateful for the input from our reviewers, Daniel McGrath, Jack Kohler, and Andrea Creighton, whose feedback greatly improved the manuscript, as well as Peter Koons for his advice on data analysis and Jonathan Maurer for preliminary data processing. We thank the Foundation for Glacier and Environmental Research and the many students, staff, and faculty of the Juneau Icefield Research Program for contributions to this research in data collection, logistical support, and preliminary data analysis. Funding from National Science Foundation award # 2239668 also supported data analysis and interpretation in this research. Any use of trade, firm or product names is for descriptive purposes only and does not imply endorsement by the U.S. Government.

References

Ballinger and 9 others (2023) Alaska Terrestrial and Marine Climate Trends, 1957-2021. *J Clim*, **36**, 4375-4391 (doi:10:1175/JCLI-D-22-0434.1)

Bigalke S and Walsh JE (2022) Future Changes of Snow in Alaska and the Arctic under Stabilized Global Warming Scenarios. *Atmosphere*, **13**, 541 (doi:10.3390/atmos13040541)

Bonnell R, McGrath D, Williams K, Webb R, Fassnacht SR, Marshall HP (2021) Spatiotemporal Variations in Liquid Water Content in a Seasonal Snowpack: Implications for Radar Remote Sensing. *Remote Sens*, **13**, 4223 (doi: 10.3390/rs13214223)

Bonnell R and 12 others (2023) Snowpack relative permittivity and density derived from near-coincident lidar and ground-penetrating radar. *Hydrol Process*, **37**, e14996 (doi:10.1002/hyp.14996)

Bradford JH, Nichols J, Mikesell TD, Harper JT (2009) Continuous profiles of electromagnetic wave velocity and water content in glaciers: an example from Bench Glacier, Alaska, USA. *J Glaciol*, **50**(51), 1-8 (doi:10.3189/172756409789097540)

Campbell, S (2024) Juneau Icefield Ground-Penetrating Radar Data – Snow and Firn. Arctic Data

Center (doi:10.18739/A2FQ9Q72N)

Clayton WS (2022) Measurement of unsaturated meltwater percolation flux in seasonal snowpack

using self-potential. *J Glaciol*, **68**(267), 25-40 (doi:10.1017/jog.2021.67)

Colbeck SC (1975) Analysis of Hydrologic Response to Rain-on-Snow. *Cold Regions Research and Engineering Laboratory*, Research Report 340

Davies B and 9 others (2024) Accelerating glacier volume loss on Juneau Icefield driven by hypsometry and melt-accelerating feedbacks. *Nat Commun,* **15**, 5099 (doi:10.1038/s41467-024-49269-y)

Gascon G, Sharp M, Burgess D, Bezeau P, Bush ABG (2013) Changes in accumulation-area firn stratigraphy and meltwater flow during a period of climate warming: Devon Ice Cap, Nunavut, Canada. *J Geophys Res*, **118**(4), 2380-2391 (doi:10.10022/2013JF002838)

Greissinger N, Mohr F, Jonas T (2018) Measuring snow ablation rates in alpine terrain with a mobile multioffset ground-penetrating radar system. *Hydrol Process*, **32**, 3272-3282 (doi:10.1002/hyp.13259)

Hansen BB and 8 others (2014) Warmer and wetter winters: characteristics and implications of an

extreme weather event in the High Arctic. *Environ Res Lett*, **9**(11), 114021 (doi:10.1088/1748-9326/9/11/114021)

Hart JK, Rose KC, Martinez K (2011) Temporal englacial water content variability associated with a rapidly retreating glacier. *Earth Surf Process Landf*, **36**(9), 1230-1239 (doi:10.1002/esp.2148)

Holland MM and Bitz CM (2003) Polar amplification of climate change in coupled models. *Clim Dyn*, **21**, 221-232 (doi:10.1007/s00382-003-0332-6)

LaChapelle ER (1954) Snow Studies on the Juneau Icefield. *Dept of Exploration and Field Research, American Geographical Society*, Report No. 9 (AD 028874)

Lundberg A, Richardson-Näslund, Andersson C (2006) Snow density variations: consequences for

ground-penetrating radar. *Hydrol Process*, **20**, 1483-1495 (doi: 10.1002/hyp.5944)

McGrath D and 7 others (2015) End-of-winter snow depth variability on glaciers in Alaska. *J Geophys Res*, **120**, 1530-1550 (doi:10.1002/2015JF003539)

McGrath D, Sass L, O'Neel S, McNeil C, Candela SG, Baker EH, Marshall H (2018) Interannual snow accumulation variability on glaciers derived from repeat extensive ground-penetrating radar surveys. *Cryosphere*, **12**, 3617-3633 (doi:10.5194/tc-12-3617-2018)

McGrath D and 6 others (2022) A Time Series of Snow Density and Snow Water Equivalent

Observations Derived From the Integration of GPR and UAV SfM Observations. *Front Remote Sens*, **3**, 886747 (doi:10.3389/frsen.2022.886747)

McNeil CJ, Sass LC, Baker EH, O'Neel S (2017) Raw Ground Penetrating Radar Data, Taku, Gilkey, Llewellyn, Tulsequah, and Norris Glaciers, Alaska, 2013-2015. U.S. Geological Survey data release (doi:10.5066/F7M043G7)

McNeil C and 6 others (2020) Explaining mass balance and retreat dichotomies at Taku and Lemon Creek Glaciers, Alaska. *J Glaciol*, **66**(258), 530-542 (doi:10.1017/jog.2020.22)

McNeil, C.,Amundson, J. M.,O'Neel, S.,Motyka, R. J.,Sass, L.,Truffer, M.,Zechmann, J. M., and Campbell, S. (2021), The imminent calving retreat of Taku Glacier, *Eos*, 102, (doi:10.1029/2021EO154856)

Meehan TG and 8 others (2021) Reconstruction of historical surface mass balance, 1984-2017 from GreenTrACS multi-offset ground-penetrating radar. *J Glaciol*, **67**(262), 219-228 (doi:10.1017/jog.2020.91)

Miège C and 12 others (2016) Spatial extent and temporal variability of Greenland firn aquifers detected by ground and airborne radars. *J Geophys Res*, **121**(12), 2381-2398 (doi:10.1002/2016JF003869)

Muñoz Sabater, J (2019) ERA5-Land monthly averaged data from 1950 to present. Copernicus Climate Change Service (C3S) Climate Data Store (CDS). DOI: 10.24381/cds.68d2bb30 (Accessed on 23-MAR-2025)

Oerlemans J and 8 others (2005) Estimating the contribution of Arctic glaciers to sea-level change in the next 100 years. *Ann Glaciol*, **42**, 230-236 (doi:10.3189/172756405781812745)

O'Neel S and 12 others (2017) Ground Penetrating Radar Data on North America Glaciers, version

2.0., July 2017: U.S. Geological Survey data release (doi:10.5066/F7M043G7)

O'Neel and 8 others (2019) Reanalysis of the US Geological Survey Benchmark Glaciers: long-term insight into climate forcing of glacier mass balance. *J Glaciol*, **65**(253), 850-866 (doi:10.1017/jog.2019.66)

Pan CG, Kirchner PB, Kimball JS, Kim Y, Du J (2018) Rain-on-snow events in Alaska, their frequency and distribution from satellite observations. *Envi Res Lett*, **13**(7), 075004 (doi:10.1088/1748-9326/aac9d3)

Pelto M and Miller MM (1990) Mass Balance of the Taku Glacier, Alaska from 1946 to 1986. *Northwest Sci*, **64**(3), 121-130

Pelto M, Kavanaugh J, McNeil C (2013) Juneau Icefield Mass Balance Program 1946-2011. *Earth Syst Sci Data*, **5**, 319-330 (doi:10.5194/essd-5-319-2013)

RGI 7.0 Consortium (2023) Randolph Glacier Inventory - A Dataset of Global Glacier Outlines, Version 7.0. Boulder, Colorado USA. NSIDC: National Snow and Ice Data Center. (doi:10.5067/f6jmovy5navz) Online access: https://doi.org/10.5067/f6jmovy5navz

Roth A, Hock R, Schuler TV, Bieniek PA, Pelto M, Aschwanden A (2018) Modeling Winter Precipitation Over the Juneau Icefield, Alaska, Using a Linear Model of Orographic Precipitation. *Front Earth Sci*, **6**(20) (doi:10.3389/feart.2018.00020)

Rounce DR and 12 others (2023) Global glacier change in the 21st century: Every increase in temperature matters. *Science*, **379**(6627), 78-83 (doi:10.1126/science.abo1324)

Schmid L, Koch F, Heilig A, Prasch M, Eisen O, Mauser W, Schweiser J (2015) A novel sensor combination (upGPR-GPS) to continuously and nondestructively derive snow cover properties. *Geophys Res Lett*, **42**, 3397-3405 (doi: 10.1002/2015GL063732)

Sihvola A and Tiuri M (1986) Snow Fork for Field Determination of the Density and Wetness Profiles of a Snow Pack. *IEEE Trans Geosci Remote Sens*, **GE-24**(5), 717-721 (doi:10.1109/TGRS.1986.289619)

St. Clair J and Holbrook WS (2017) Measuring snow water equivalent from common-offset GPR records through migration velocity analysis. *Cryosphere*, **11**, 2997-3009 (doi: 10.5194/tc-11-2997-2017)

Sold L, Huss M, Eichler A, Schwikowski M, and Hoelzle M (2015) Unlocking annual firn layer water equivalents from ground-penetrating radar data on an Alpine glacier. *The Cryosphere*, **9**, 1075-1087 (doi:10.5194/tc-9-1075-2015)

Techel F and Pielmeier C (2011) Point observations of liquid water content in wet snow – investigating methodical, spatial, and temporal aspects. *Cryosphere*, **5**, 405-418 (doi:10.5194/tc-5-405-2011)

Thornton TF (2010) Haa Leelk'w Has Aani Saax'u/Our Grandparents' Names on the Land. University of Washington Press (ISBN: 9780295988580)

Tiuri M, Sihvola A, Nyfors E, Hallikaiken M (1984) The complex dielectric constant of snow at microwave frequencies. *IEEE J Ocean Eng*, **9**(5), 377-382 (doi: 10.1109/JOE.1984.1145645)

Webb RW, Jennings KS, Fend M, Molotch NP (2018) Combining Ground-Penetrating Radar With

Terrestrial LiDAR Scanning to Estimate the Spatial Distribution of Liquid Water Content in Seasonal Snowpacks. *Water Resour Res*, **54**, 10339-10349 (doi: 10.1029/2018WR022680)

Webb RW, Wigmore O, Jennings K, Fend M, Molotch NP (2019) Hydrologic connectivity at the hillslope scale through intra-snowpack flow paths during snowmelt. *Hydrol Process*, **34**, 1616-1629 (doi:10.1002/hyp.13686)

Webb RW, Musselman KN, Ciafone S, Hale KE, Molotch NP (2022) Extending the vadose zone: Characterizing the role of snow for liquid water storage and transmission in streamflow generation. *Hydrol Process*, **36**, e14541 (doi: 10.1002/hyp.14541)

Winski D and 10 others (2018) A 400-Year Ice Core Melt Layer Record of Summertime Warming in the Alaska Range. *J Geophys Res Atmos*, **123**(7), 3594-3611 (doi:10.1002/2017JD027539)

Xu M, Yang Q, Hu X, Liang K, Vihma T (2022) Record-breaking rain falls at Greenland summit controlled by warm moist-air intrusion. *Environ Res Lett*, **17**(4), 044061 (doi:10.1088/1748-9326/ac60d8)

Zheng J, Jia G, Xu X (2022) Earlier snowmelt predominates advanced spring vegetation greenup in Alaska. *Agric For Meteorol*, **315**, 108828 (doi:10.1016/j.agrformet.2022.108828)

Table 1. Dates and types of ground-truth data and GPR surveys. Surface correction was applied to the sites in 2012 where GPR and GT measurements were not collected on the same day.

Year	Ground-truth (GT)	GT type	GT date	GPR date	Surface Correction (cm)
2012	DG1	Snow pit	14 July	14 July	
	SWB2	Snow pit	18 July	15 July	+14.6
	TKG3	Snow pit	16 July	17 July	-5.6
	TKG7	Snow pit	21 July	22 July	-5.0
	NWB1	Snow pit	22 July	22 July	
	C161	Snow pit	23 July	23 July	
2021	SWB2	Snow core	10 July	10 July	

TKG5	Snow pit	13 July	13 July
TKG4	Snow pit	13 July	13 July
TKG3	Snow pit	13 July	13 July
MC1	Snow core	13 July	13 July
TKG7	Snow pit	15 July	15 July
C161	Snow pit	15 July	15 July

Table 2. Comparison of the range of annual-accumulation snow water equivalent (SWE) for 2012 and 2021 based on the maximum, average (± 1 standard deviation (s.d)), and minimum values for calculated relative permittivity (ε_s) for the shared extent of radar surveys.

Year		$\varepsilon_{s,\,min}$	$\overline{\varepsilon_s}$ - 1 s.d.	$\overline{\varepsilon_s}$	$\overline{\varepsilon_s}$ + 1 s.d.	$\varepsilon_{s,\,max}$
2012	SWE	315 ± 98	298 ± 93	286 ± 89	275 ± 85	278 ± 86
	ε_s	*2.06*	*2.29*	*2.48*	*2.68*	*2.62*
2021	SWE	253 ± 104	226 ± 95	193 ± 80	163 ± 68	160 ± 66
	ε_s	*2.11*	*2.49*	*3.56*	*4.63*	*5.11*

Figure 1:

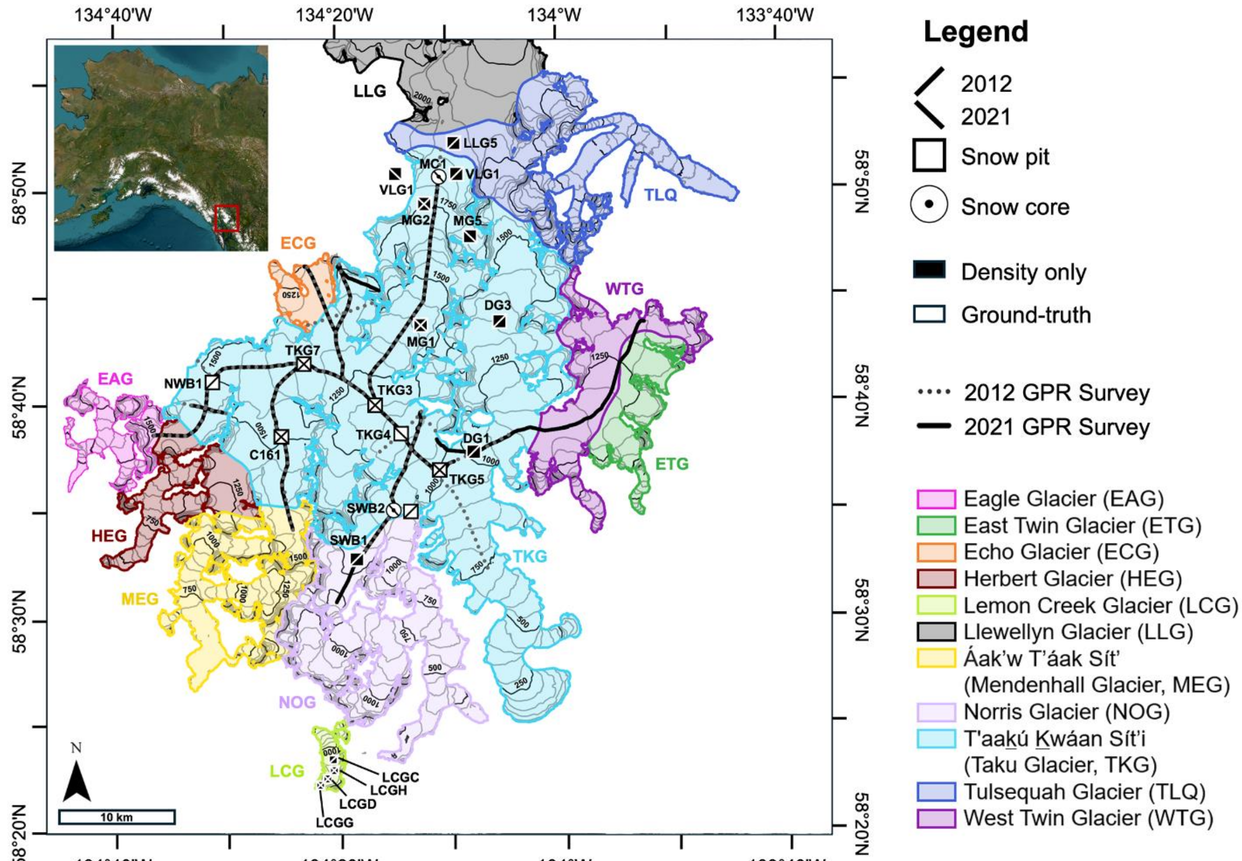
134°40'W
134°20'W
134°W
133°40'W
58°50'N
58°40'N
58°30'N
58°20'N
LLG
LLG5
MC1
VLG1
VLG1
MG2
MG5
TLQ
ECG
DG3
MG1
WTG
TKG7
NWB1
EAG
TKG3
TKG4
DG1
C161
TKG5
ETG
HEG
SWB2
SWB1
TKG
MEG
NOG
LCG
LCGC
LCGH
LCGD
LCGG
N
10 km
Legend
2012
2021
Snow pit
Snow core
Density only
Ground-truth
2012 GPR Survey
2021 GPR Survey
Eagle Glacier (EAG)
East Twin Glacier (ETG)
Echo Glacier (ECG)
Herbert Glacier (HEG)
Lemon Creek Glacier (LCG)
Llewellyn Glacier (LLG)
Áak'w T'áak Sít'
(Mendenhall Glacier, MEG)
Norris Glacier (NOG)
T'aak̲ú K̲wáan Sít'i
(Taku Glacier, TKG)
Tulsequah Glacier (TLQ)
West Twin Glacier (WTG)

Figure 2:

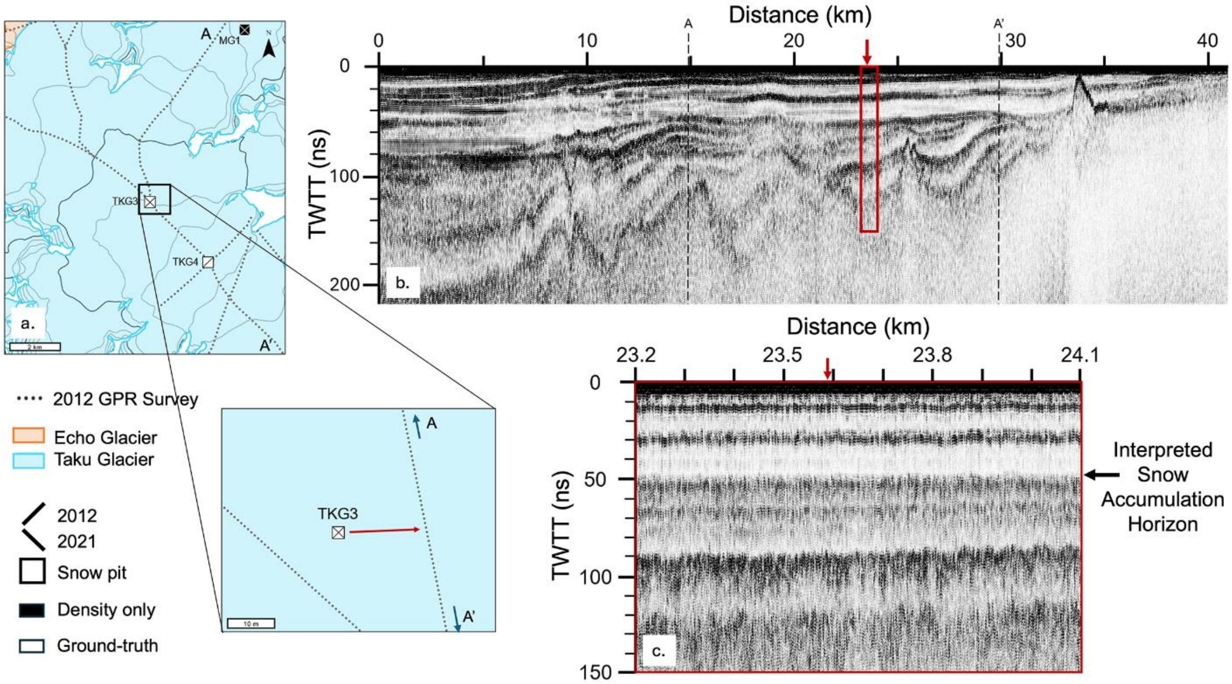

Figure 3:

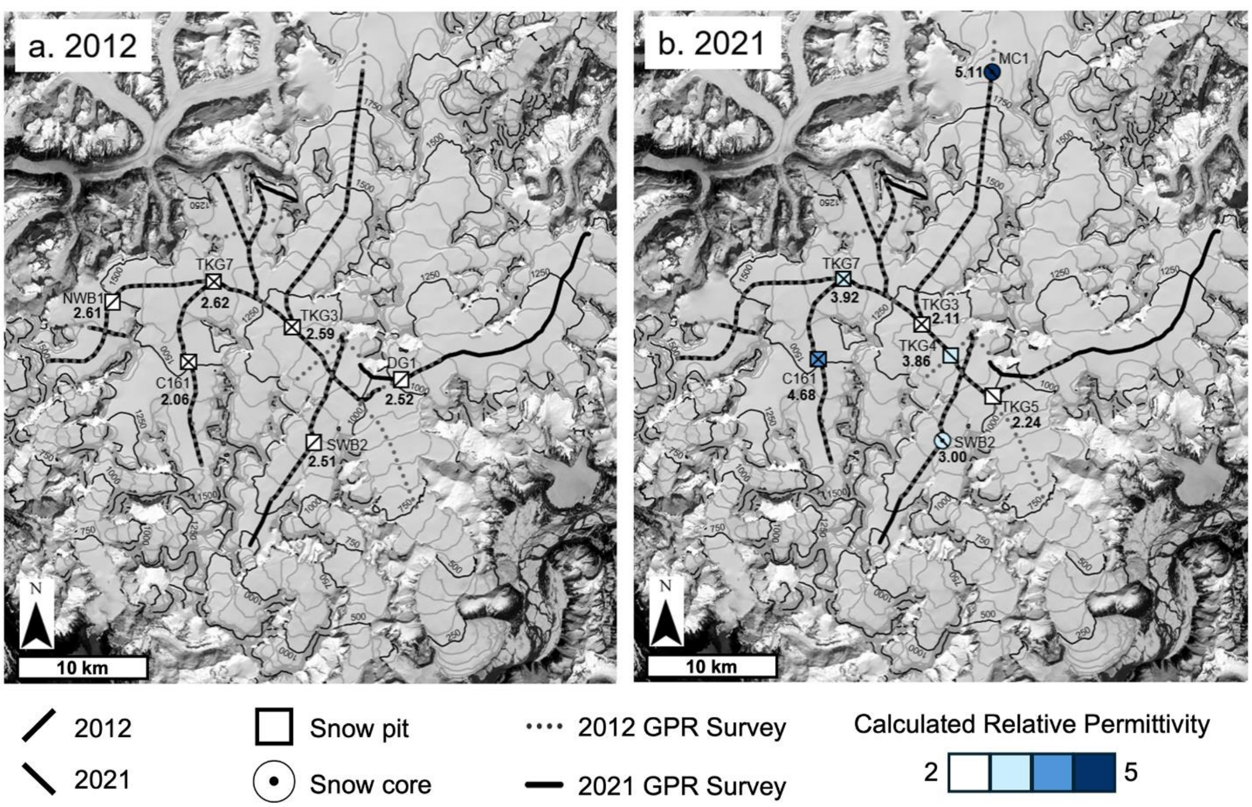

Figure 4:

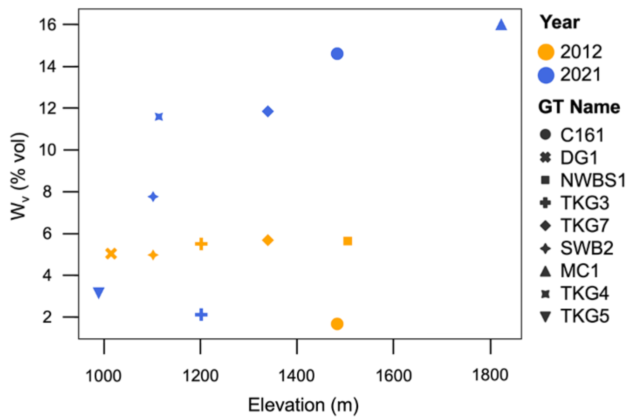

Figure 5: